LA-UR- 98-3460

Approved for public release; distribution is unlimited.

Title: ANALYSIS OF THERMAL ISSUES ASSOCIATED WITH THE PRE-AMPLIFIER MODULES IN THE NATIONAL IGNITION FACILITY

Author(s): Kin L. Lam, LANL, ESA-EA

Submitted to: DOE/ASCI/Richard A. Lesar

Los Alamos
NATIONAL LABORATORY

DISCLAIMER

Analysis of Thermal Issues Associated with the Pre-Amplifier Modules in the National Ignition Facility

Kin L. Lam
Group ESA-EA
Los Alamos National Laboratory
Los Alamos, NM 87545

1. Introduction

The design of the National Ignition Facility (NIF) calls for a desired temperature field of 20.00±0.28°C throughout the facility. This design requirement is needed to prevent degradation of the operating performance and net yield of the NIF by heat loads generated within the facility. In particular, the potential interference of waste heat from the lighting fixtures and equipments such as the electronics racks, and pre-amplifier modules (PAMs), and its impact on the operational performance of the laser beam transport tubes and optical alignment components must be evaluated. This report describes the thermal analyses associated with the PAMs. Evaluation of thermal issues for the other equipments is discussed elsewhere.

2. Heat Dissipation Characteristics of a PAM

The PAM is a multi-functional, highly integrated two-stage amplifier package. Each PAM unit contains an optics bay, which is housed in an optical support structure (OSS). An electronics bay (e-bay) is placed on top of the OSS. Figure 1 illustrates the major assemblies in a PAM. The e-bay is made up of an electronic chasis with rack mounted components and is covered by aluminum sheets. The electronic components in

the e-bay collectively produce 628 W of waste heat, according to PAM prototype power consumption measurements.

The waste heat generated in the e-bay must be removed. Forced air flow at a rate of 130 ft^3/min (0.061 m^3/s) through the e-bay cools the electronic components and chasis. The air flow is provided by an inlet and outlet fans, which are located at each end of the e-bay. Before the warm air exits the e-bay, it is passed through an air-water exchanger, which uses about 1 gal/min of actively controlled flow of water at 45°F (7°C) to cool the air back to the facility nominal air temperature of 20°C.

In this thermal study, our goal is to determine the influence of the waste heat generation in the e-bays on the temperature of the air above the PAMs and inside the OSS. It is assumed (and was supported by prototype experiments) that the air-water heat exchanger effectively cools the exit forced air from the e-bay before it returns to the facility. Our focus is then on the amount of heat generated in the e-bay that is not removed by the forced air flow. That amount of heat will be transmitted through the sheet-metal cover of the e-bay to warm the air above.

In the following, we will describe two computational models used for this analysis. These models address separately the thermal effects of the PAM waste heat generation on the facility (laser-bay) and OSS air temperatures.

3. Computational Models and Boundary Conditions

Two PAM units are typically stacked one on top of another in the pre-amplifier support structure. Figure 2 depicts schematically such an arrangement, showing the

e-bay and OSS of each PAM. Outlined in red are the two main computational models used in this study. Model A is used to analyze the effect of the e-bay waste heat generation on the air above the upper PAM unit, whereas Model B is used to study the effects on the air in the OSS.

In both Models A and B, the e-bay (3.42 m long, 0.182 m high, and 0.710 m wide) is idealized as consisting of all solid at the bottom and free air space at the top. The solid volume at the bottom represents the combination of all the components in the e-bay which act as flow obstacles. It is assumed that the solid obstacle volume occupies 80% of the total e-bay volume, leaving 20% free volume for the forced air flow to go through. This assumption leads to an average air velocity of 2.4 m/s (based on volumetric flow rate of 0.061 m^3/s divided by the idealized e-bay free-space cross-sectional area of 0.0258 m^2), which is consistent with prototype air velocity measurements in various locations within the e-bay.

We used the computational fluid dynamics code, CFX Version 4.2 [Ref. 1], to analyze the fluid flow and heat transfer phenomena present in the current PAM thermal problems. Two-dimensional, steady-state calculations were carried out for Models A and B. The ambient air, forced flow inlet, and enthalpy reference temperatures are all set to 20°C. In the following, we will describe the geometry, boundary conditions, and spatial discretization for the two models.

Figure 3 shows the overall dimensions, material distribution, and boundary conditions used in Model A, which consists of the upper e-bay and the laser bay air above it. Volume occupied by a 0.635 cm thick foam-board insulation on top of the sheet

metal is included so that cases with and without insulating the top of the e-bay can be studied. Note that the vertical scales for the sheet metal and e-bay air are expanded. The horizontal dimension, which represents the length of the e-bay, is 3.42 m. The e-bay free-space height is 3.6 cm, and the sheet metal is 0.229 cm thick. The vertical dimension of 3 m for the outside (i.e., laser bay) air was judged to be high enough such that the constant pressure boundary condition at the top boundary does not affect the development of the thermal plume caused by the heated sheet metal.

In addition to the top boundary, the left and right boundaries of the outside air volume are also under constant pressure boundary condition, which will allow air to flow in or out depending on the fluid dynamics developed inside the computational domain.

For the e-bay air volume, the left boundary is specified with a constant mass inflow (74 g/s of air at 20°C) boundary condition that corresponds to 130 ft^3/min. On the right boundary, the mass outflow (or alternatively constant pressure) boundary condition is specified. On the bottom boundary of the e-bay air volume, a constant heat flux of 258.6 W/m^2 (628 W divided by the bottom wall area of 2.428 m^2) is specified as this boundary also represents the top wall of all the e-bay components (which produce the waste heat) lumped together, which are not modeled directly here.

For spatial discretization in Model A, 100 uniformly spaced cells are used in the horizontal direction. In the vertical direction, 20 cells are used for the e-bay air, 3 for the sheet metal, 8 for the insulation (if exists), and 95 for the outside air. The total number of cells is 12,600. The cell sizes in the vertical direction are chosen such that more cells bunch up near solid walls to better resolve boundary layers.

Model B consists of the lower e-bay and the upper OSS, separated by an air space in between. Figure 4 illustrates the overall dimensions, material distribution, and boundary conditions used in this model. The e-bay, sheet-metal, insulation material (if exists) and overall horizontal dimensions are the same as in Model A. The OSS is 0.787 m high, and has a steel bottom wall that is 0.318 cm thick. The OSS is modeled as a closed volume in which air flow is not allowed in or out. The air space between the OSS and e-bay is 0.25 m high.

Boundary conditions for the e-bay air region are the same as in Model A. Similarly, the left and right boundaries of the outside air are under constant pressure boundary condition. For the OSS, the top wall is specified with the adiabatic boundary condition. The left and right walls of the OSS are specified with a heat flux boundary condition that models cooling of the walls by natural convection of the outside (laser-bay) air. This boundary condition is derived as follows:

$$q''_w = k\frac{\partial T_w}{\partial x} = h(T_\infty - T_w) \tag{1}$$

$$k\frac{\partial T_w}{\partial x} + hT_w = hT_\infty \tag{2}$$

where T_w, q''_w are the temperature and heat flux at the wall, k is the thermal conductivity of air in the OSS, T_∞ is the ambient air temperature (20°C), and h is the heat transfer coefficient that represents the heat removal capability of the ambient air via natural convection at the vertical OSS walls. The value of h chosen for the natural convection boundary conditions is 1.428 W/m^2-K, which is determined from the following correlation

developed by Churchill and Chu (Ref. 2) based on a temperature difference (ΔT) of 1°C and the OSS height (L) of 0.787 m:

$$Nu_L \equiv \frac{hL}{k} = 0.68 + 0.67 Ra_L^{1/4} \left[1 + (0.492/\mathrm{Pr})^{9/16}\right]^{-4/9}, \text{ where} \tag{3}$$

$$Ra_L \equiv \frac{g\beta \Delta T L^3}{\alpha \nu} \tag{4}$$

Note that this correlation is applicable to both laminar and turbulent natural convection on vertical isothermal surfaces. The ΔT value of 1°C assumed above is verified to be roughly the calculated temperature difference between the vertical OSS boundaries and the ambient air (see Section 4.3).

The overall horizontal spatial discretization, as well as the discretization of the e-bay air region, sheet metal, and insulation in Model B are the same as in Model A. The air space between the e-bay and OSS is meshed with 80 computational cells vertically while the OSS is meshed with 65 cells. Again, the distribution of cells is such that they converge toward solid boundaries to better resolve momentum and thermal boundary layers. The total number of cells used in Model B is 17,900.

In both Models A and B, conducting solid models are used to invoke conjugate heat transfer with the adjacent fluid (air) regions. Modeled conducting solid materials include the aluminum sheet metal, insulation material, and OSS steel wall. The thermal properties of these conducting solids are summarized in Table 1.

Table 1. Physical properties of conducting solids specified in CFX calculations.

Conducting Solid	Thermal Conductivity (W/m/°C)	Specific Heat Capacity (J/kg/°C)	Density (kg/m^3)
Sheet Metal (Aluminum)	237	905	2707
Steel	43	473	7801
Foam-board Insulation	0.01	1000	790

The calculations for Models A and B were performed both with and without radiation modeling. Radiation heat transfer was modeled in the CFX calculations with the Shah discrete transfer method, using 12 rays and one radiation call per five fluid and heat flow iterations. Surface emissivities for all inflow, outflow, and pressure boundaries are set to unity to represent a non-reflective radiation boundary condition. The other boundaries (solid surfaces) have emissivity values listed in Table 2.

Table 2. Emissivities of various solid surfaces specified in CFX calculations.

Material	Aluminum Sheet Metal	Steel	Foiled Foam-Board Insulation	E-Bay Solid Components
Surface Emissvity	0.09	0.66	0.07	0.5

All four boundaries of the OSS are assumed to be steel surfaces with an emissivity of 0.66. The emissivity value of 0.5 for the e-bay solid components is an approximation for a fictitious surface of the idealized solid volume that lumps all the flow obstacles together.

All of the calculations invoked the standard k-ε turbulence model. The fluid flow was modeled as incompressible, and buoyancy was modeled with the Boussinesq approximation.

4. Results

In all of the calculations, convergence to steady-state solutions was considered achieved when the residuals of all the nonlinear outer iteration equations decreased by at least three orders of magnitude between the second and last iterations. The nonlinear equations include two momentum, a pressure (mass), and enthalpy equations, as well as transport equations for k and ε. Because energy balance is especially important for the current problem, the enthalpy conservation equation was iterated four times in each outer iteration loop. Convergence of this equation was aided with false time stepping at a step size of 0.1 s. Global energy balance check for all calculations indicated that the energy was conserved to within 0.1%.

It was found that using double-precision for the current calculations was essential in obtaining well converged solution for the enthalpy equation within a reasonable number of iterations (about 2000). This is because even small temperature differences (e.g., 0.1 K in the absolute temperature scale, which is used by CFX computations, of about 300 K) are significant for the current problem and the temperature solutions in most regions are approximately the same (293 K or 20°C). Although the double-precision option needed

about 50% more memory than single-precision in these calculations, the more accurate computations led to shorter CPU times and more straightforward convergence strategies.

Most calculations converged to acceptable steady-state solutions within 10 hours of CPU time. In the following, calculation results for Models A and B will be discussed separately.

4.1 Model A Results

The purpose of the Model A calculations is to assess the thermal plume above the upper e-bay that develops as a result of the waste heat generated by the electronic components. We will discuss calculations without radiation modeling first, then those with radiation modeling. The effects of insulating the top of the sheet metal will also be discussed.

Figure 5 shows the calculated temperature contours and velocity vectors when radiation modeling was not included, for both the cases with and without insulation. Note that the temperature scale was chosen with a maximum at 20.28°C and minimum at 20°C. Therefore, regions with temperatures above 20.28°C all appear red on the contour plots. A thermal plume above the e-bay is clearly shown. If we define the plume by the 20.23°C temperature contour line, then the plume height is 0.94 m for the case without insulation, and is 0.39 m for the case with insulation. The thermal plume is caused by the amount of waste heat that is not carried away by the forced flow inside the e-bay. The fractional amount of waste heat escaping the e-bay through the sheet metal is 2.3% for the case without insulation and 0.7% for the case with insulation.

Figure 5 also shows the flow patterns. The warm rising air that forms the thermal plume above the sheet metal is replenished by cooler air flowing into the computational domain from both the left and right sides. The maximum velocity magnitude within the plume is 11 cm/s for the case with no insulation and 10 cm/s for the case with insulation. Velocity vectors within the e-bay are not shown in Fig. 5, because the e-bay height is too small compared to the air above it and because the vectors inside the e-bay would overwhelm those defining the thermal plume. The calculated velocity in the e-bay exhibits a typical profile for a turbulent forced channel flow, with a maximum velocity of 2.78 m/s at the center for all cases (i.e., Models A and B, with and without insulation and radiation modeling).

Other temperature results are that the sheet metal reaches a maximum of 24°C for the case without insulation and 25°C for the case with insulation. In both cases, the maximum temperature at the bottom wall which gives off the waste heat is 41°C, and the forced air flow exits the e-bay with a temperature profile of 38°C at the bottom and 25°C the top.

We performed a calculation to assess the effect of a higher waste heat generation, in which the power was increased by 10% from 628 W to 691 W. Figure 6 shows the resulting thermal plume for this higher-power case, together with the nominal power case with no insulation. It can be seen that the thermal plume is higher by about 40% (1.3 m compared to 0.94 m).

Figure 7 shows the temperature contours and velocity vectors with radiation modeling included in the calculations. It can be seen that the thermal plume is weaker

than in the above case in which radiation modeling was not included. This is because radiation from the top of the sheet metal (or insulation) to the constant-pressure boundaries (which were assumed to be black-body heat sinks with an emissivity of unity) provide an additional cooling mechanism. The plume height is now 0.38 m for the case without insulation, and is 0.21 m for the case with insulation. The percentages of the total power escaping the e-bay through the sheet metal for the cases without and with insulation are 3.3% and 0.9%, respectively. The maximum velocity within the plume is 6 cm/s for the case without insulation, and is 4 cm/s for the case with insulation. The sheet metal maximum temperature is about the same as in the case without radiation modeling (i.e., 24°C without insulation and 25°C with insulation). The maximum temperature at the bottom wall is 40°C, and the maximum temperature of the forced air flow at the exit is 37°C, for both cases with and without insulation. Table 3 lists the important results for Model A.

Table 3. Summary of results for Model A

	No Radiation Modeling		With Radiation Modeling	
	No Insulation	With Insulation	No Insulation	With Insulation
Plume Height (m)	0.94	0.39	0.38	0.21
% Total Power Through Sheet Metal	2.3%	0.7%	3.3%	0.9%

4.2 Model B Results

With Model B, we study the effects of the waste heat generated within the lower e-bay on the air temperature inside the OSS above. As in Model A, calculation results for cases with and without radiation modeling, and with and without insulation on top of the sheet metal will be presented.

Figure 8 shows the calculated temperature contours and velocity vectors when radiation modeling was not included, for both the cases with and without insulation. Note that the scale for the temperature contours has a maximum of 22°C. As in Model A, a thermal plume develops in the air above the e-bay, which is caused by the warm sheet metal. In the current case, however, the plume is deflected horizontally as it hits the bottom wall of the OSS. As a result, the flow pattern in the air space between the lower e-bay and the upper OSS is such that warm air leaves the left and right boundaries at the top while cool air is drawn in at the bottom across the same boundaries. The fractional amount of the total waste heat that escapes the e-bay through the sheet metal is 1.6% for the case without insulation and 0.6% for the case with insulation.

As can be seen in Fig. 8, two convection loops occur inside the OSS, with warm air rising near the middle, deflecting sideways at the top wall, then flowing downward along the two cooled side walls. The average temperature of the air in the OSS is 21.3°C without insulation and 20.7°C with insulation. About 1 W and 0.54 W, respectively, of heat enters the OSS from the bottom for the cases with no insulation and with insulation.

Other results, such as the maximum temperatures of the sheet metal, of the bottom wall giving off the waste heat, and of the exit forced flow of air, are very similar to those in Model A.

Figure 9 shows the temperature contours and velocity vectors with radiation modeling included in the calculations. Note the change in the maximum temperature on the contour color scale to 23°C. A general observation is that with radiation modeling included, the air within the OSS becomes slightly warmer than in the case with no radiation modeling. This is because the top and side walls (especially the top wall, which was specified with an adiabatic boundary condition), with an emissivity value of 0.66, absorb as well as reflect energy back into the computational domain. Similar flow patterns develop both inside the OSS and in the air space between the e-bay and OSS, as in Model A. But the average temperature of the air inside the OSS in this model is 22.1°C without insulation and 21.7°C with insulation. The percentages of the total power escaping the e-bay through the sheet metal for the cases without and with insulation are 3.3% and 0.9%, respectively. Table 4 lists the major results for Model B.

Table 4. Summary of results for Model B.

	No Radiation Modeling		With Radiation Modeling	
	No Insulation	With Insulation	No Insulation	With Insulation
OSS Air Temperature Rise (°C)	1.3	0.7	2.1	1.7
% Total Power Through Sheet Metal	1.6%	0.6%	1.8%	0.7%

5. Lumped-Parameter Analysis

All of the CFX calculations for Models A and B above were 2D, an assumption which enables simplification (and speedup) of the calculations compared to full 3D modeling. The 2D assumption was chosen because it is conservative, in the sense that the actual thermal effects of the waste heat generated in the e-bay are expected to be less severe than those calculated because the third dimension, which was not modeled, may provide additional pathways of air flow and walls for cooling. For Model B, this conservative assumption led to an OSS air temperature rise of 1–2°C, as shown by the CFX results discussed above. This relatively high temperature rise warrants additional analysis. One approach is to extend Model B to 3D and perform more complex CFX calculations. We will not pursue this method. Rather, a simpler lumped-parameter analysis is presented here, with the purpose of assessing how conservative the 2D CFX results are for Model B by ignoring the OSS walls in the third dimension.

In this lumped-parameter study, we assume that the OSS air volume and the inner walls are at a single temperature (i.e., boundary layers and thermal gradients at the walls are ignored). We will denote this temperature as an increase from the ambient (20°C), namely ΔT_{OSS}. This temperature rise is determined by the balance of the energy coming in from the bottom wall, q_{in}, against the loss of energy through the vertical walls by natural convection of the outside air, q_{out}. The CFX calculations for Model B indicated that q_{in} is about 1.0 W. The rate of energy lost, q_{out}, can be related to ΔT_{OSS} as follows:

$$q_{out} = hA_{total}\Delta T_{OSS}, \quad \text{where} \tag{5}$$

h is a heat transfer coefficient for natural convection at the temperature difference ΔT_{OSS}, and A_{total} is the total vertical wall area, which includes the side and end walls. The side walls are defined as those that are parallel to the forced flow in the e-bay, which were ignored in the 2D CFX calculations. Therefore, we have

$$A_{total} = A_{sides} + A_{ends} \tag{6}$$

$$A_{sides} = 7.083 \text{ m}^2 \tag{7}$$

$$A_{ends} = 1.118 \text{ m}^2 \tag{8}$$

$$A_{total} = 8.201 \text{ m}^2 \tag{9}$$

The heat transfer coefficient h depends on ΔT_{OSS} through a correlation involving the Rayleigh number, which is given in Eqs. (3-4). By requiring that q_{out} be equal to q_{in}, which is known, and explicitly writing h as a function of ΔT_{OSS} in Eq. (5), we have

$$h(\Delta T_{OSS})A_{total}\Delta T_{OSS} = q_{in}, \quad \text{where} \tag{10}$$

The only unknown in the above equation is ΔT_{OSS}. However, an iterative procedure is required for its solution because the function $h(\Delta T_{OSS})$ as given by Eqs. (3-4) are nonlinear. However, starting from an initial guessed temperature difference of 1°C, one can easily obtain a converged solution for the set of equations (3), (4), and (10) within several iterations. The solution is

$$\Delta T_{OSS} = 0.138°C \tag{11}$$

and the corresponding values for Ra_L and h are 6.5×10^6 and 0.886 W/m^2-°C, respectively.

The temperature rise inside the OSS calculated here, at 0.138°C, is considerably lower than that calculated in the 2D CFX Model B (which gives 1–2°C). However, the present lumped-parameter analysis under-predicts the OSS temperature because it ignores the inner wall boundary layers. In reality, the vertical walls are cooler than the bulk air in the OSS, thus lowering the natural convection heat loss capability (driving force) at the walls. Therefore, one cannot conclude based on this analysis that the OSS temperature rise is as low as 0.138°C. However, the lumped-parameter method is still useful in providing an estimate of the effect of ignoring the two side walls in the CFX calculations in Model B, as discussed in the following.

Comparing Eqs. (7) and (9), one can see that the side wall area represent 86% of all the available vertical wall area for natural convection heat transfer to the outside air. This large fraction of the surface area was ignored in the 2D CFX calculations. To estimate the effect of leaving out the side wall area, we repeat the above lumped-

parameter study using only the end wall area. In other words, we solve Eq. (10) with a slight change in variables:

$$h(\Delta T'_{OSS})A_{ends}\Delta T'_{OSS} = q_{in}, \quad \text{where} \tag{12}$$

$\Delta T'_{OSS}$ represents the temperature rise if only the end walls are included for heat transfer. Solution of Eq. (12), in conjunction with Eqs. (3–4), gives

$$\Delta T'_{OSS} = 0.683°C \tag{13}$$

Now the effect of only having the end walls available for natural convection heat transfer can be quantified by the following factor

$$F_{2D} = \Delta T'_{OSS} / \Delta T_{OSS} = 5.0 \tag{14}$$

If one assumes that this conservative factor for the temperature rise also applies approximately to the CFX calculations, then one can estimate that the 2D Model B results are also conservative by roughly a factor of 5 (as a result of ignoring the side walls). If all three dimensions are included in the modeling, the OSS air temperature rise will be 5 times less than 1–2°C, equal to 0.2–0.4°C.

The temperature rise can be further reduced by insulating the steel bottom wall of the OSS, across which escaped waste heat from the e-bay below enters. Without insulation, the temperature drop across the 0.318-cm thick steel wall is of the order of (10^{-5})°C, which is negligible, for q_{in} = 1.0 W across the OSS bottom wall surface area of 2.428 m^2. If foam-board insulation with a thickness of 0.635 cm is applied to the bottom steel wall, then a temperature drop of 0.26°C will occur across the insulation for the same

heat flux. Therefore, insulating the bottom wall of the OSS can reduce the temperature rise in the OSS air by up to 0.26°C.

6. Conclusions

Based on the Model A results, the 20.28°C contour plume height is 0.94 m, which can be reduced to 0.39 m if the sheet metal is insulated with 0.635-cm thick foam board material. Based on the results of Model B and related lumped-parameter analyses, the average temperature rise of the air inside the OSS is 0.2 to 0.4°C, depending on whether the sheet metal is insulated. If the bottom of the OSS is insulated with the same foam-board material, then the OSS air temperature rise can be reduced by up to 0.26°C.

We recommend that the sheet metal covering the e-bays and the bottom wall of the upper OSS be insulated to mitigate the thermal effects of the escaped waste heat on the air above the PAM units and on the air inside the OSS.

References

[1] CFX 4.2 Flow Solver User Guide, 1998, Computational Fluid Dynamics Services, Harwell Laboratory, Oxfordshire OX11 0RA, United Kingdom.

[2] Churchill, S. W., and Chu, H. H. S., 1975, "Correlating Equations for Laminar and Turbulent Free Convection from a Vertical Plate," *Int. J. Heat Mass Transfer*, Vol. 18, pp. 1323-1329.

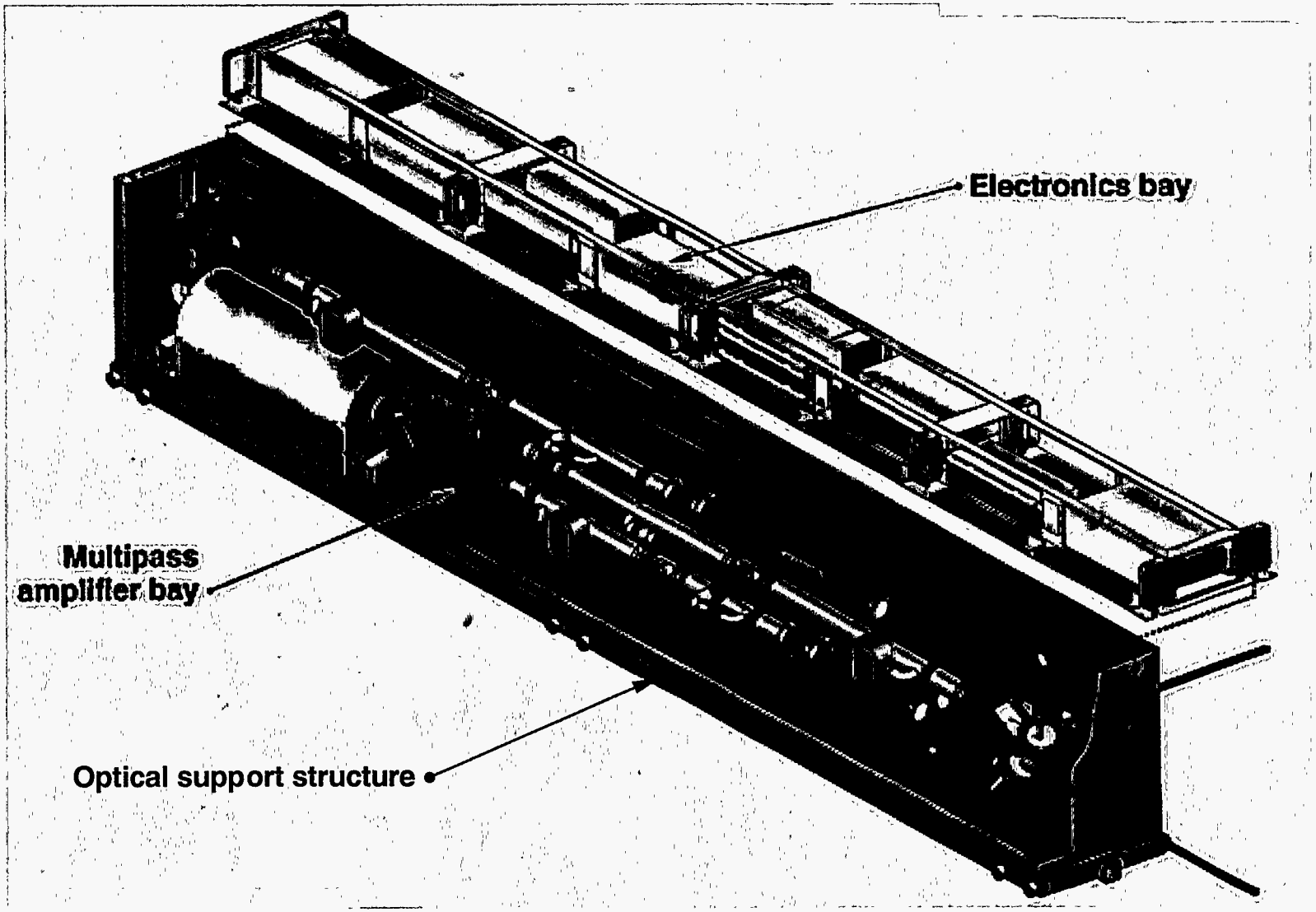

Figure 1. Major assemblies in a PAM. The sheet metal covering the electronics bay and the front cover of the optical support structure are not shown.

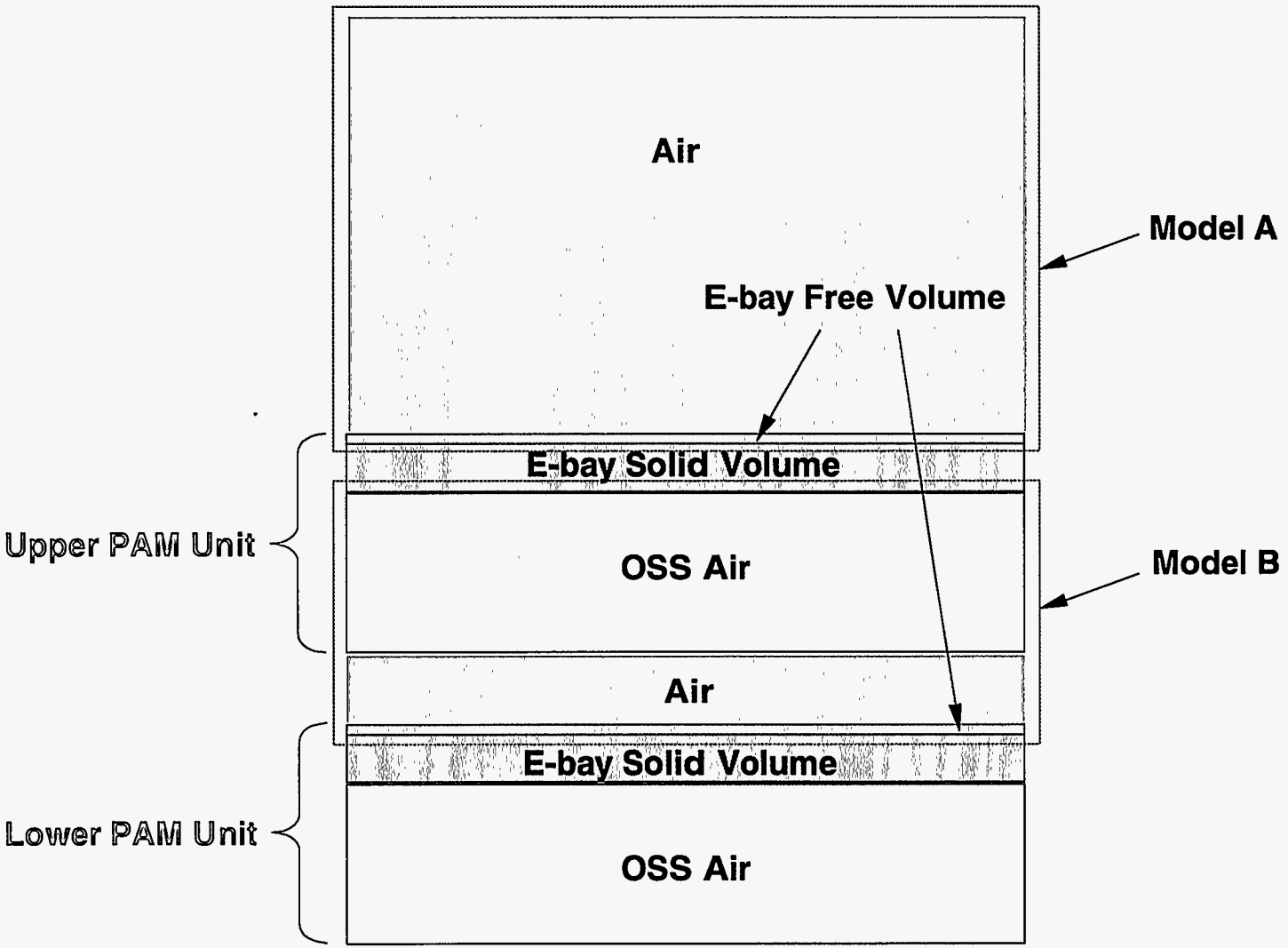

Figure 2. Schematic drawing of two PAM units depicting Models A and B used in thermal analysis studies. Note: Vertical dimensions not to scale.

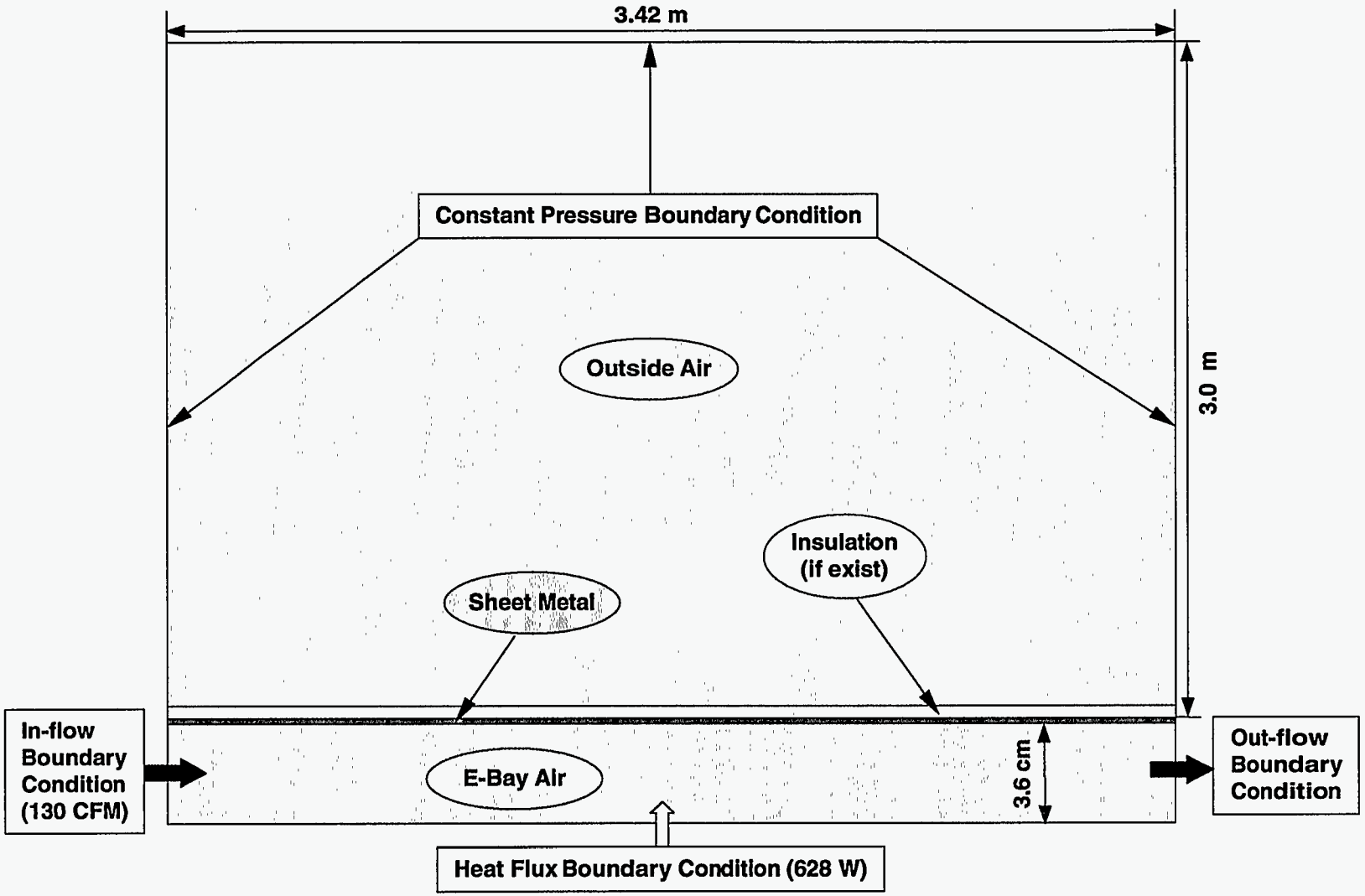

Figure 3. Overall dimensions, material distribution, and boundary conditions used in Model A, which consists of the upper e-bay and the laser bay air above it. Note: Vertical dimensions not to scale.

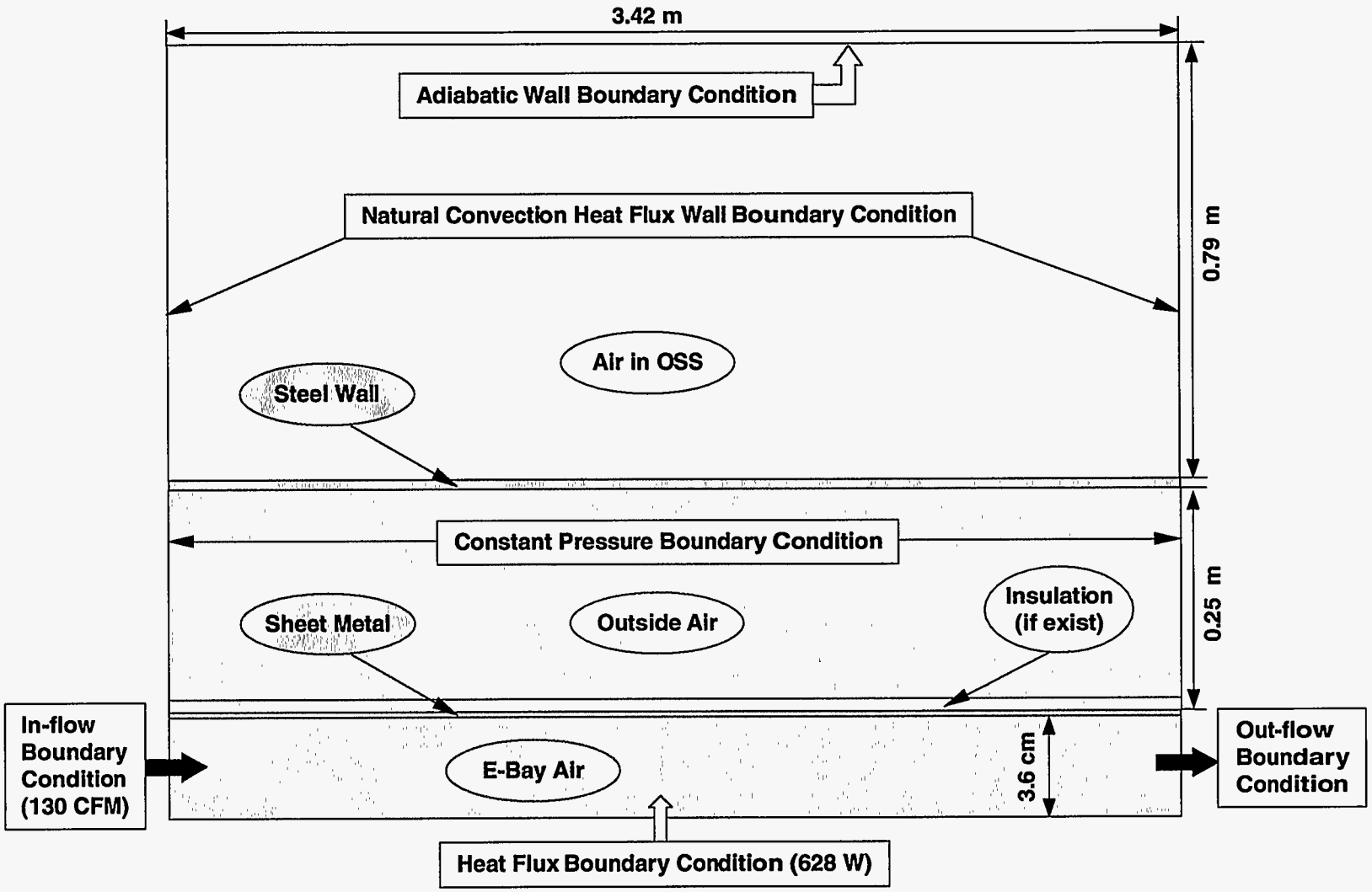

Figure 4. Overall dimensions, material distribution, and boundary conditions used in Model B, which consists of the lower e-bay and the upper OSS separated by an air space. Note: Vertical dimensions not to scale.

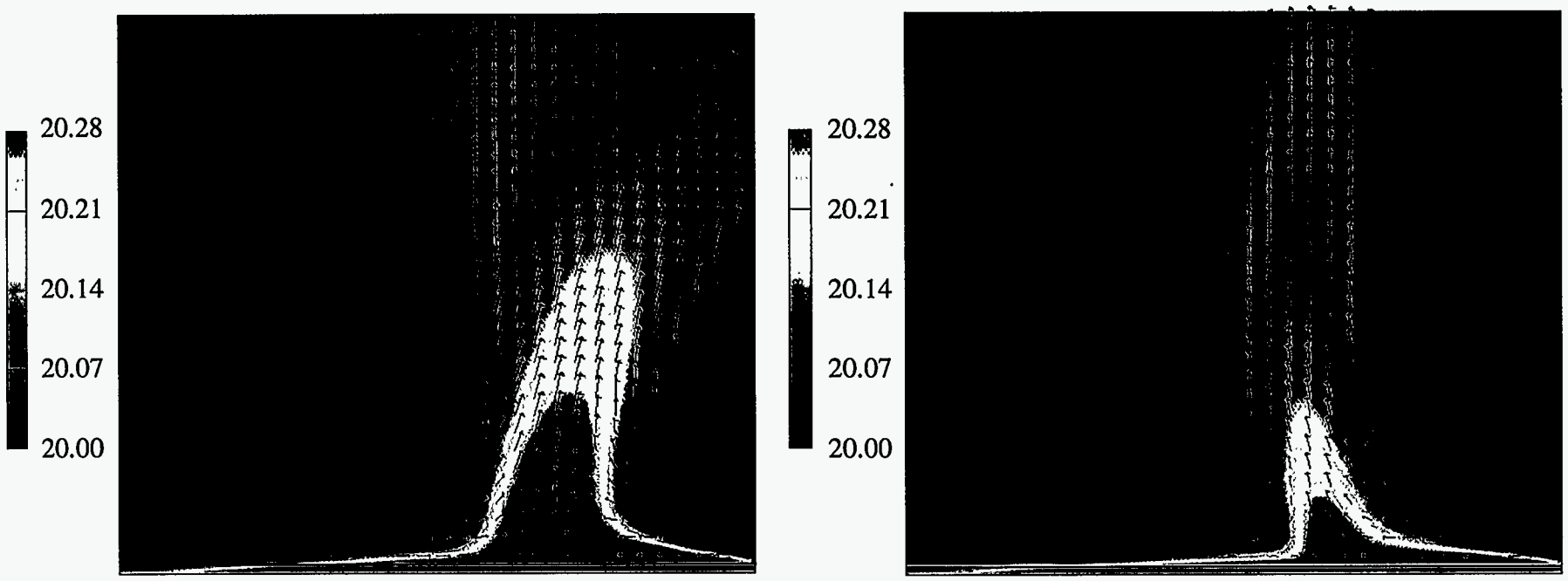

Figure 5. Calculated temperature contours and velocity vectors for Model A.
Left: no insulation (base case); right: with insulation.

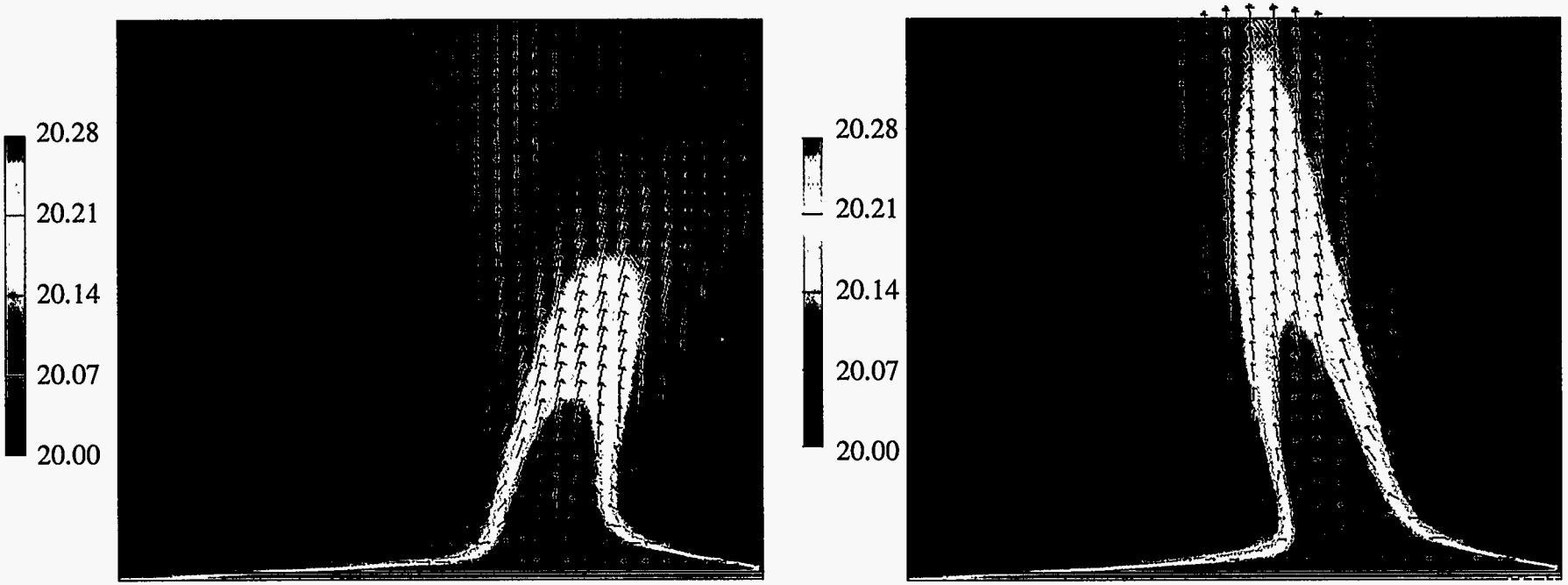

Figure 6. Calculated temperature contours and velocity vectors for Model A, comparing two waste heat levels. Left: 628 W (base case); right: 691 W.

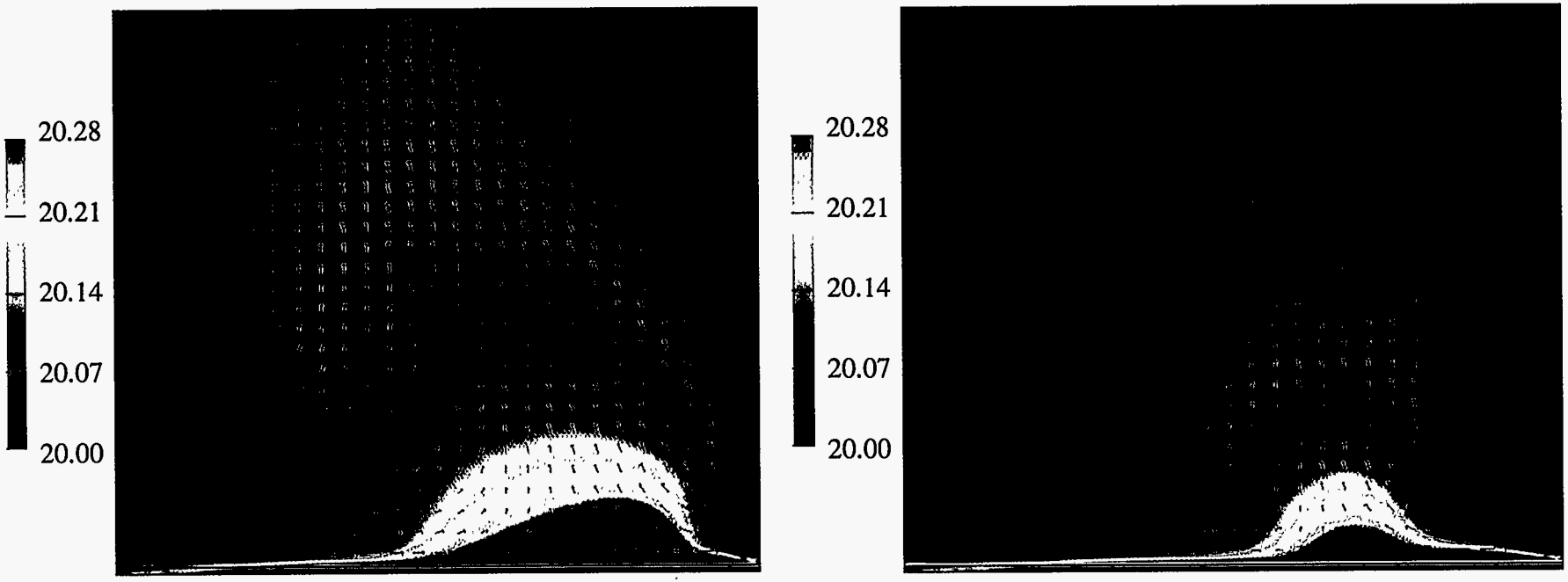

Figure 7. Calculated temperature contours and velocity vectors for Model A, with radiation modeling. Left: no insulation; right: with insulation.

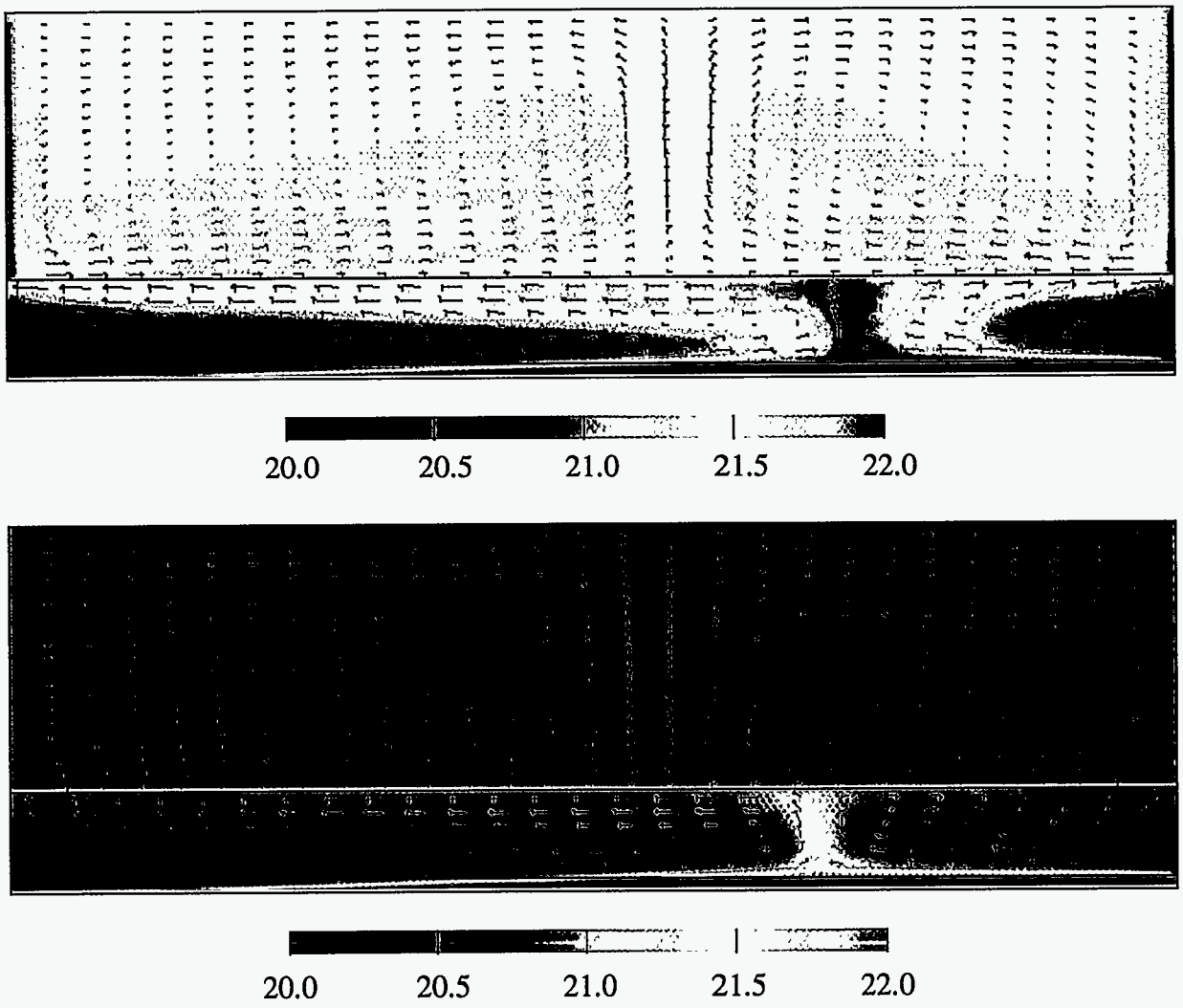

Figure 8. Calculated temperature contours and velocity vectors for Model B.
Top: no insulation; bottom: with insulation.

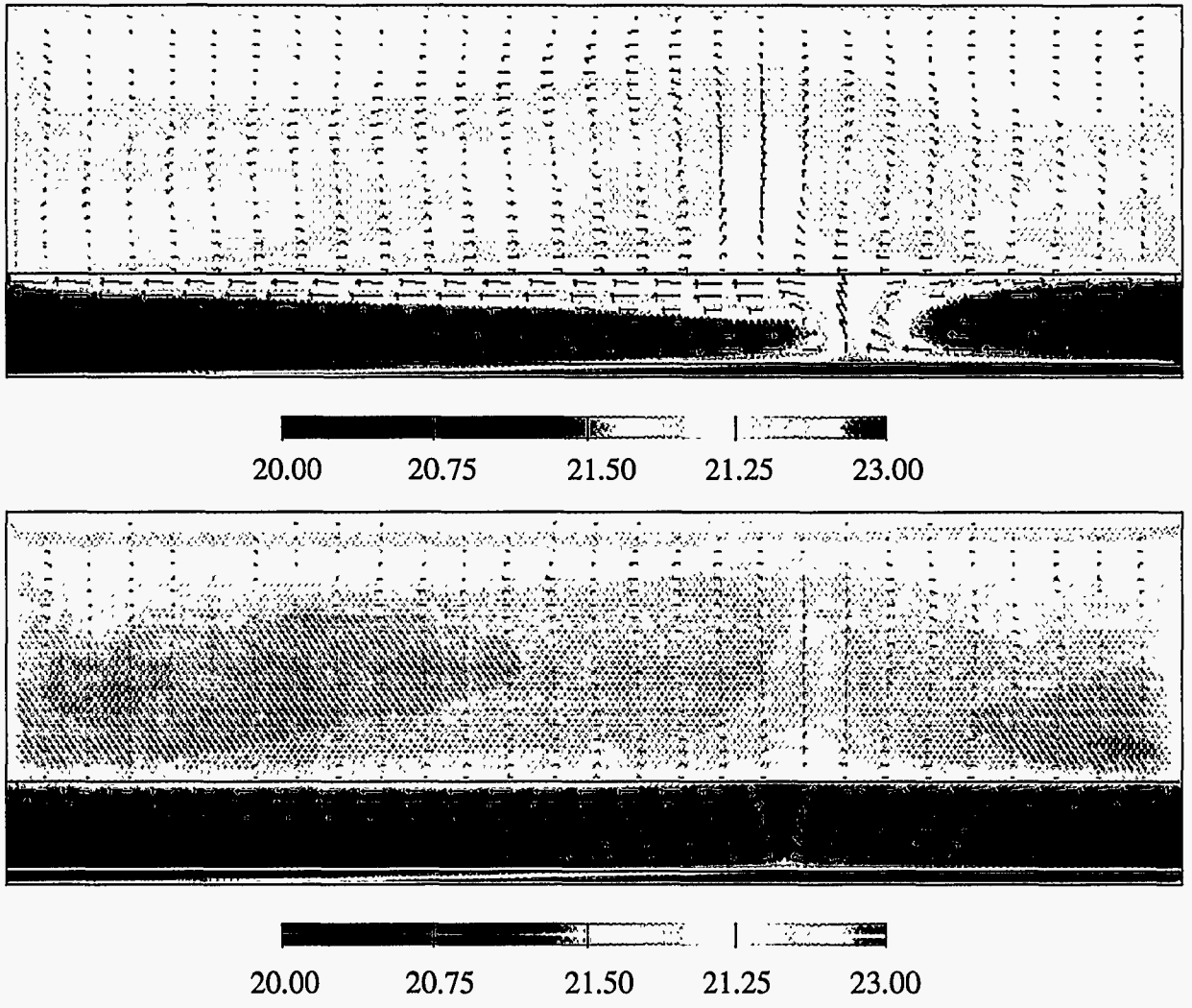

Figure 9. Calculated temperature contours and velocity vectors for Model B, with radiation modeling. Top: no insulation; bottom: with insulation.